

BARC

NEWSLETTER



भाभा परमाणु अनुसंधान केंद्र
BHABHA ATOMIC RESEARCH CENTRE



IN THIS ISSUE

- Development and adoption of Low Sodium Glass frit for Vitrification of High Level Radioactive Liquid Waste at Tarapur
- Indigenous Development of Carbon Aerogel Farad Super-capacitors and Applications in Electronic circuits
- Measurement of mechanical properties of a PHWR operated pressure tube using an in-house developed 'In situ Property Measurement System (IProMS)'
- Numerical Simulations to Evaluate Different Approaches for scaling up of Packed Bed Membrane Reactor for HI Decomposition

In the Forthcoming Issue

1. Phase transformation and deformation studies in Zr based Alloys
by K V Mani Krishna, et al.
2. The exciting world of the neutrino and the India based Neutrino Observatory
by V.M. Datar, et al.
3. Stress Analysis and Free Vibration of Functionally Graded Plates with Higher Order Shear and Normal Deformations Theories
by Jha, et al.
4. Tsunami Warning System based on Seismic Data
by S Mukhopadhyay, et al.
5. Numerical Simulations to Evaluate Different Approaches of Scale-up of Packed Bed Membrane Reactor for HI Decomposition
by Nitesh Goswami, et al.

CONTENTS

<i>Editorial Note</i>	ii
Visit	
• The Prime Minister visits BARC	iii
Brief Communications	
• Indigenous Switch-Routers for Dependable Video Surveillance Networks	v
• Development of Rare Earth Based Products	vi
Research Articles	
• Development and adoption of Low Sodium Glass frit for Vitrification of High Level Radioactive Liquid Waste at Tarapur <i>T.P. Valsala, et al</i>	1
• Indigenous Development of Carbon Aerogel Farad Super-capacitors and Applications in Electronic circuits <i>Shantanu Das and N. C. Pramanik</i>	5
Technology Development Articles	
• Measurement of mechanical properties of a PHWR operated pressure tube using an in-house developed 'In situ Property Measurement System (IPromS)' <i>S. Chatterjee, et al</i>	11
• Numerical Simulations to Evaluate Different Approaches for scaling up of Packed Bed Membrane Reactor for HI Decomposition <i>Nitesh Goswami, et al</i>	18
News and Events	
• Nisargruna Plant Inaugurated at RRCAT Campus, Indore	23
• Conference on "75-years of Nuclear Fission Present status and future perspectives"	24
BARC Scientists Honoured	26

Editorial Committee**Chairman**

Dr. S.K. Apte,
Director, Bio-Science Group

Editor

Dr. K. Bhanumurthy
Head, SIRD

Associate Editors for this issue

Mr. G. Venugopala Rao, APPD
Dr. S.M. Yusuf, SSPD

Members

Dr. R.C. Hubli, MPD
Dr. D.N. Badodkar, DRHR
Dr. K.T. Shenoy, ChED
Dr. A.P. Tiwari, RCnD
Dr. S.M. Yusuf, SSPD
Dr. A.K. Tyagi, ChD
Mr. G. Venugopala Rao, APPD
Dr. C.P. Kaushik, WMD
Dr. G. Rami Reddy, RSD
Dr. S. Kannan, FCD
Dr. A.K. Nayak, RED
Dr. S.K. Sandur, RB&HSD
Dr. S.C. Deokatney, SIRD

From the Editor's Desk.....

Welcome to the fourth issue of the BARC Newsletter for the year 2014. This issue carries four interesting articles and two Brief Communications.

The Honourable Prime Minister of India, Shri. Narendra Modi has made his first visit to BARC, Mumbai on 21st July 2014 and a brief account of this important visit is included in the first section of this report.

An important work on the development of rare earth-transition metal based alloy powers such as Sm-Co and its method of fabrication was discussed in one of the brief communication. Indigenous development of switch-routers for dependable video surveillance has been described on another short communication.

BARC is involved in Hydrogen production by thermo-chemical splitting of water through the IS process. Different approaches have been evaluated to scale up the PBMR (Packed Bed Membrane Reactor), for the decomposition of Hydrogen Iodide. This evaluation has been carried out using numerical simulations.

Cyclic ball indentation is an emerging technique in the area of alternate methods for estimation of properties of materials. BARC has developed an 'In situ Mechanical Property Measurement System (IProMS)', suitable for Zr-2.5Nb pressure tubes is described in one of the articles.

Finally, your contributions are important to further enrich our newsletter and I request to send your contributions.



Dr. K. Bhanumurthy
On behalf of the Editorial Committee

The Prime Minister visits BARC

The Honorable Prime Minister of India, Shri Narendra Modi, made his first visit to BARC at Trombay, Mumbai on 21st July, 2014. He was received by Dr. R.K Sinha Secretary, DAE and Chairman, AEC and welcomed by Shri Sekhar Basu, Director, BARC. The Prime Minister had a discussion with Dr. R.K. Sinha, Shri Sekhar Basu, Shri S. S. Bajaj, Chairman, AERB and other senior officers and scientists of BARC. As a token of respect, Dr. R.K. Sinha presented a 3D model of Cirus and Dhruva reactors to the Honorable Prime Minister.

Shri R.C. Sharma, Director, Reactor Group welcomed the Chief Guest on his arrival at the Dhruva research reactor. Dr. R.K. Sinha demonstrated the Dhruva Model and explained its functioning to the Prime Minister. Dr. Sinha also enlightened the Prime Minister about the various important and critical components of the reactor. He also briefed him on DAE's extensive research & development DAE's

contributions in the areas of health care, especially cancer treatment, food security, solid waste management, water purification and public awareness programmes. The Prime minister also witnessed the operation of Dhruva from its control room.

During his visit to various facilities at BARC and referring to the occasion of the Diamond Jubilee of DAE, the Prime Minister urged DAE to draw up a programme of year long celebrations, which would highlight the achievements of DAE, particularly to the public at large. The Prime Minister was apprised of the safety measures adopted by DAE for radiological protection of both man and environment and India's excellent record in this regard. Prime Minister expressed his appreciation for the extraordinary achievements of the Indian scientific community in one of the most complex and challenging fields of science and technology.



Dr. R.K. Sinha, Chairman, AEC, Shri Sekhar Basu, Director, BARC briefing the Prime Minister during the Poster Exhibition

Indigenous Switch-Routers for Dependable Video Surveillance Networks

Electronics and Instrumentation Group

Video-surveillance represents a security sensitive application and usually consists of number of geographically distributed cameras (fixed and PTZ type) connected to a farm of high performance servers (for display, recording, storage) through computer network. Currently all network devices are of foreign origin leading to cyber security concerns in critical applications. Now, we have an indigenous solution for dependable and secure surveillance network.

Carrier Ethernet based switch-routers designed by IIT-Bombay are being manufactured under license by ECIL as ECR series products. E&I Group, BARC is involved in adding value to this path-breaking new technology through enhancements and evaluation studies so as to increase its penetration in security sensitive and strategic applications. ECR routers with their proprietary routing protocols are well-suited for closed group communication where cyber-security is a concern. This, along with low latency and low power make them especially attractive option for integrating video-surveillance networks spanning 10's of Kms and thousands of cameras.

Currently, three models (Fig.1: ECR-100/1000/1010) are available. Together, they provide both copper and optical Ethernet ports and support 10/100/1000 Mbps speeds as well as 10Gbps Ethernet or OTN. A light-weight Network Management System(NMS) helps in configuration, operation, monitoring and maintenance of the network. The network is "completely managed"- all communication parameters are a-priori configured from NMS. Only the configured nodes are allowed to communicate with other configured nodes and the traffic is limited

to the provisioned bandwidth. This feature greatly enhances security since access to network is restricted to configured, authorized users/ devices.

Salient features of ECR based networks are given below.

- Provides a high level of protection against DoS (Denial of Service) attacks.
- Inherent topology security provides data-origin authentication.
- Configuration change and download is authorized and authenticated before being accepted and is maintained on power-on/off.
- Replay of control plane traffic for configuration is protected through timeout of authentication and session tokens
- Any fault in the network is detected and switchover to pre-defined redundant path occurs within 50msec and is annunciated on NMS.

E&I Group, BARC has successfully integrated a prototype Video Surveillance system around these ECR switch-routers. Specific functions were added to the devices to optimize their performance in a video-surveillance application. These include Internet Group Management Protocol (IGMP) for dynamic join and leave for multicast group and provision to handle burst of traffic from cameras without incurring delays and freeze-frames. Fig.2 shows the screenshot of display workstation for 3 camera network.

ECR routers are well-suited for demanding video-surveillance applications; it offers an indigenous, dependable, secure and economical alternative for security sensitive installations while planning their video-surveillance systems.



Fig.1: ECR100, ECR1000 and ECR1010



Fig. 2: VMS screenshot of 3 cameras

Development of Rare Earth Based Products

Materials Group

Permanent magnets based on rare earth-transition metal intermetallics are the basis of ever increasing number of commercial and scientific applications, including electric motors, NMR scanners, voice coil motors, magnetic bearings, loudspeakers, magnetic resonance, wind-mills, compact discs, data storage devices, actuators for robotics and flight control, etc. The advantage of permanent magnets in these applications is their ability to exhibit high level, constant magnetic fluxes without applying an external magnetic field or electrical current. Samarium-cobalt based magnets have been prepared with high energy product and excellent coercive force and are ideally compact and suitable for highly efficient machines and components in which higher operation temperature, higher corrosion and oxidation resistance are crucial.

Rare earth-transition metal based alloy powders, such as Sm-Co have been prepared by reduction-diffusion (R-D) method using calcium as a reductant by

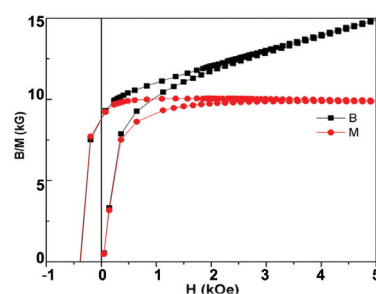
calciothermic reduction of samarium oxide in presence of cobalt under argon atmosphere. SmCo_5 was prepared in kilogram quantities. The desired phases as revealed by X ray diffraction studies showed the formation of required phase when the reduction was carried out with excess of Ca as compared to stoichiometric requirement, in the temperature range of 1100-1200°C. Almost 95% CaO was removed by leaching the product with water. For further decrease of residual calcium, leaching with buffer solution containing ammonia and organic acid was necessary. Fine control of pH was found to be necessary to bring down the calcium content below 2000 ppm in the final product without disturbing the magnetic phases. The R-D product with higher Sm and lower Ca shows much better residual magnetization and energy product, which are essential requirements for a good permanent magnet. Due to its inherent high energy product, Sm-Co based permanent magnets have been several applications in our nuclear energy program.



SmCo_5 alloy prepared by R-D process



Magnets prepared from SmCo_5 alloy



Magnetization curve of a product containing 37% Sm and 2000 ppm Ca

Development and adoption of Low Sodium Glass frit for Vitrification of High Level Radioactive Liquid Waste at Tarapur

T.P. Valsala, S. Chattopadhyay, R.V. Jayan, N.L. Sonar, P.K. Mishra, Vinit Kumar Mittal, Vaishali De, D.A. Thakur, R.K. Sah, Amrita Dhara, Soumya Sen, R.K. Dubey, I. Vishwaraj and Y. Kulkarni

Tarapur Waste Management Plants, Nuclear Recycle Board,
Bhabha Atomic Research Centre, Tarapur

Abstract

High level Liquid Waste (HLW) is generated during the reprocessing of spent nuclear fuel which is used to recover uranium and plutonium. More than 99% of the fission product activity generated during the burning of nuclear fuel in the reactor is present in HLW. For the efficient management of HLW by vitrification, sodium borosilicate glass has been adopted worldwide. Sodium oxide acts as modifier in glass matrix and variation in its concentration may vary the properties of the glass and hence the melter parameters. The HLW presently used for vitrification has higher concentration of sodium. As the composition of the base glass is fixed the concentration of Na in the HLW is one of the limiting factors for the waste loading for the vitrification process. Present article gives a brief account of the formulation of a base glass frit with lower sodium content and the feedback after implementing in the vitrification plant.

Introduction

Reprocessing of the spent nuclear fuel is an integral part of the Indian Atomic Energy programme, as the Pu produced during the first stage of power generation can be separated and utilized in the second stage. However, the reprocessing of the spent nuclear fuel results in the generation of radioactive liquid wastes. The high level radioactive waste (HLW) generated during the burning of the fuel in the reactor contains more than 99% of the fission product activity and requires utmost consideration owing to the presence of long-lived radionuclides. Sodium borosilicate glass has been adopted as a solid matrix for immobilization of the HLW world wide [1]. Joule heated ceramic melter is used for the vitrification of high level radioactive waste in Advanced Vitrification System at TWMP Tarapur [2]. In joule heated ceramic melter, HLW along with base glass in the form of glass nodules is used instead of slurry containing raw glass forming chemicals.

A five component base glass composition based on $\text{SiO}_2\text{-B}_2\text{O}_3\text{-Na}_2\text{O-Fe}_2\text{O}_3\text{-TiO}_2$ system was studied and being used at AVS at Tarapur. In the vitrification process of HLW, the mass ratios of the glass matrix system play an essential role in the encapsulation of various hazardous elements present in the HLW. The properties and structure of the glass are strongly dependent on the composition, mainly on the $\text{SiO}_2/\text{Na}_2\text{O}$ mole ratio and SiO_2 content [4-5]. The concentration of non-bridging oxygen (NBO) increases with decreasing $\text{SiO}_2/\text{Na}_2\text{O}$ mole ratio and this has direct impact on decreasing the glass formation temperature as well as chemical durability of the glass. During vitrification of HLW sodium is getting added in the product glass both from waste as well as from base glass frit. Since the glass forming chemicals are added in the form of preformed glass nodules, there is no scope for changing the base glass composition when the HLW composition changes. This restricts the waste loading

Table 1: Properties of new base glass nodules procured

Properties	Specified range	Analysed range
Bead dia, mm	2-3	2-3
Bead density, gm/cc	1.4 - 1.8	1.60-1.70
Breaking strength of a bead, kg	12-15	15-23
Pouring temperature (range), °C	1100 -1150	1100
Attrition characteristics (Fines generation on vigorous shaking for 2.0 hours)	< 0.5%	< 0.2 %

and hence the through put of the melter whenever there is high sodium content in the waste. The HLW presently taken for vitrification has higher concentration of sodium which limits the waste loading in to the product glass. Hence it is required to have a base glass composition with lower sodium content which has formation temperature suitable for the joule melter. A brief account of the formulation of a base glass frit with lower sodium content for vitrification of HLW having higher sodium content is given below. The feedback after adopting it in the vitrification process is also given.

Formulation of base glass frit composition having lower sodium content

Different glass frit formulations having lower sodium content were prepared [6]. These glass formulations were evaluated for formation temperature and glass transition temperature. Out of these compositions, the one which is compatible for AVS joule melter operation with respect to glass formation temperature (1100°C) and glass transition

temperature (551°C) was selected for further studies. Product glass samples with varying waste oxide loading were prepared and studied using the new base glass formulation and simulated HLW.

Procurement of base glass nodules and evaluation

Based on the laboratory studies, base glass nodules having lower sodium content were procured from CGCRI and samples from the bulk supply was analysed for different physical properties and chemical composition. The physical properties (Table-1) and the chemical composition (Table-2) of the nodules were well within the specified limits.

Product glass was prepared using this glass nodules and simulated HLW in the laboratory and evaluated (Table-3). DTA and XRD analysis of product glass were carried out to see glass transition temperature (T_g) and extent of crystallization respectively (Fig. 1 & 2). XRD scan of the heat treated product glass (72 hours nucleation at 650°C and 168 hours heat treatment at 750°C) was also taken to see the decay

Table 2: Chemical compositions of base glass nodules procured

Oxide	Existing composition	Target new composition, wt %	Acceptable Range wt (%)	New base glass nodules analysed, wt%
SiO ₂	48.0	52.3	50.0 - 53.0	52.5 – 52.9
B ₂ O ₃	26.5	24.0	19.0 – 25.0	22 - 23
Na₂O	11.5	9.5	8.5 – 9.5	9.3 – 9.7
TiO ₂	9.5	9.5	8.0 - 9.5	9.0 – 9.5
Fe ₂ O ₃	4.5	4.7	4.0 - 4.7	4.2 - 4.3

Table 3: Joule melter parameters during vitrification operations

	Average Pouring rate, Kg/min	Pouring Temp, °C	Glass poured after initiating stoppage of pouring action, Kg	ACPC Power, KW	DAC Value in side the cell during pouring, DAC
VWP with existing glass nodules	1.91	807 °C	4.9	2.4	\hat{a} = BDL \hat{a} = 4.6
VWP with low sodium glass nodules	1.96	843°C	5.3	1.8	\hat{a} = BDL \hat{a} = 2.3

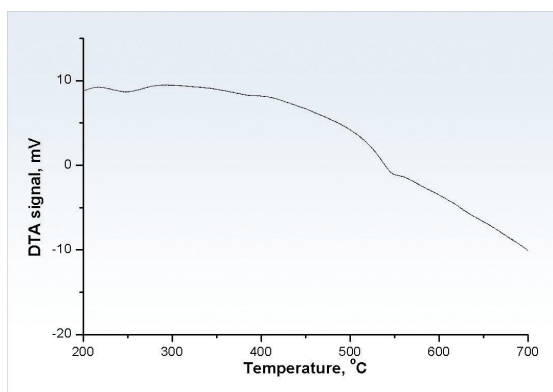


Fig. 1: DTA scans of the product glass

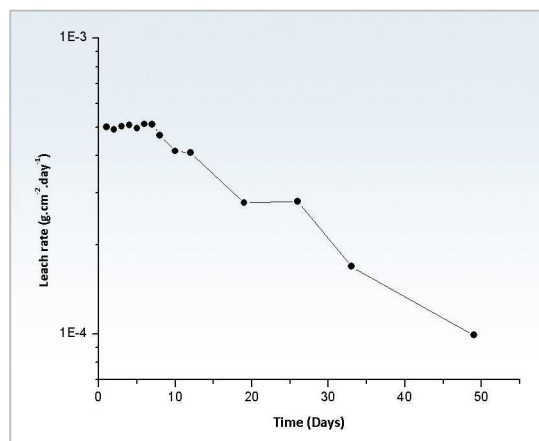


Fig. 3: Leaching pattern of Na from product glass

heat effect on the product glass (Fig. 2). The chemical durability of glass was measured by standard leach method [7] in which glass is crushed in to powder of -16 to +25 ASTM mesh size and packed in SS mesh.

The Tg value (546°C) and density (2.66g/cc) of the prepared product glass are comparable to the existing

AVS product glass. The XRD scan of product glass is amorphous showing that the extent of crystallization in the glass sample is negligible. The product glass remained amorphous even after heat treatment at 750°C for 7 days. Fig. 3 shows the logarithm of normalized leach rate for Na ions as a

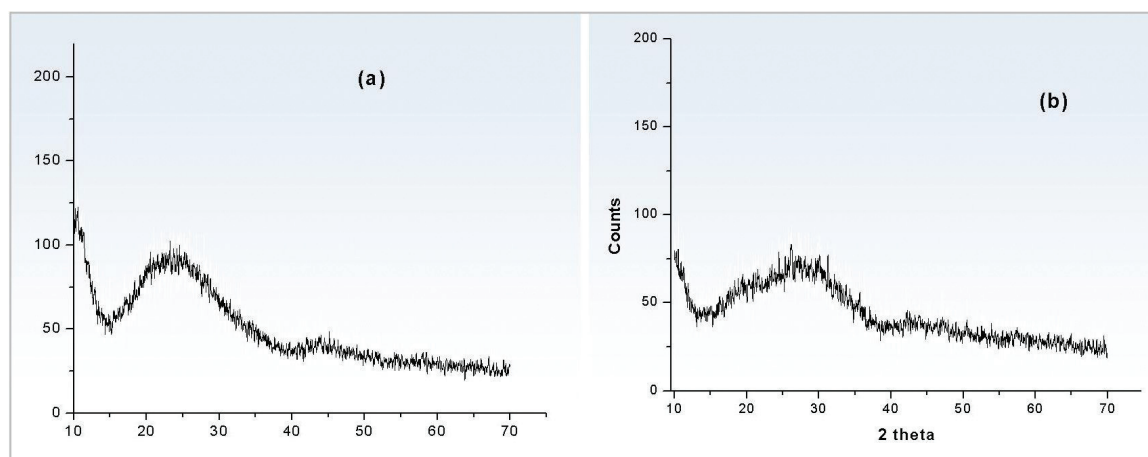


Fig. 2: XRD scans of product glass (a) before and (b) after heat treatment

function of time. The average leach rate ($9.90 \times 10^{-5} \text{ g.cm}^{-2}.\text{day}^{-1}$) obtained after 50 days leaching is comparable with the existing product glass data.

Adoption of the low sodium base glass nodules for vitrification operation at AVS

After evaluating the base glass nodules and simulated product glass in the laboratory safety clearance was obtained to use the glass nodules for vitrifying HLW in AVS joule melter. Ten numbers of vitrification operations using these glass nodules has been completed producing 1100 kgs of vitrified waste product. This has increased the waste loading in to the product glass by 25% (by volume). The operation parameters of joule melter during these operations are comparable to the operations with existing glass nodules (Table -3).

Conclusion

Adoption of base glass nodules having lower sodium content has resulted in increased waste oxide loading in to vitrified waste product, which in turn reduced the space requirement for interim storage and long term disposal of vitrified waste product.

Acknowledgement

Authors are thankful to Shri. S.Pradhan, Chief Superintendent, TNRPO, NRB, for the support

provided during the work. Authors thank Shri. M.S. Sonavane for the help provided during the procurement of the Low sodium glass nodules from CGCRI. We acknowledge the contribution of Dr. J. G. Shah and Smt. Annie Joseph for the XRD analysis of the samples.

References

1. M. I. Ojovan and O. K. Karlina, *Radiochim. Acta* **34** (1992) 97-100.
2. K.Raj, K.K.Prasad, N.K.Bansal, *Nucl. Engg. Design*, 236 (2006).
3. Vogel, W. *Glass Chemistry*, Springer, Berlin, 1994.
4. Ehrt, D. & Ebeling, P. *Glass Technol.*, 2003, 44, 46.
5. Rawson, H. *Inorganic glass forming systems*, Academic Press, London, 1967.
6. De Vaishali, Sah R.K, Mishra P.K., Sonar N.L., Valsala T.P. and Sonavane M.S, in proceedings of THERMANS-2008, Kalpakkam, 2008, p 398.
7. Hanawalt et al., *Anal. Chem.*, 10, 475 (1938) (PDF # 01-0927).

Indigenous Development of Carbon Aerogel Farad Super-capacitors and Applications in Electronic circuits

Shantanu Das

RCSDS, Reactor Control Division

and

N. C. Pramanik

Aerogel Division, Centre for Materials for Electronics Technology (C-MET),
Thrissur

Abstract

Indigenous R&D efforts are taken to develop carbon aerogel based super-capacitors also known as electric double layer capacitors (EDLC). They possess wide application potentials in many electronics industry including applications in power electronics, UPS, high speed communication systems requiring 'burst currents', powering electronics in airborne defence strike systems, powering sensors in remote boarder areas, electric vehicles, pulsed power devices and Micro-Grid power systems, solar-energy to electrical energy conversion systems (for improving store/load performance and reducing the size of battery based systems), which are important R&D programmes of our immediate interest toward the national needs. Here we report the major achievements on the development of aerogel super-capacitors and applications in electronic circuits. Carbon aerogel supercapacitors of cell capacitance in the range of 1-35 F@/2.5V were developed using carbon aerogel as the active electrode materials, and some demonstration circuits were made.

Introduction

Supercapacitors, commonly known as electric double layer capacitors (EDLC) are considered as efficient energy storage device and have received large research interest because of its increasing demand for various electronics applications requiring high power densities and moderate energy densities¹⁻². Due to increase in demand for miniaturization and high performance of memory backup devices, high power electronic components etc., carbon aerogel as active electrode material of supercapacitors has received immense attraction due to its unique micro-structure and physical properties^{1,3-5}. It is important to mention here that EDLC are composed of a pair of easy polarisable electrodes, having electrode surface area, a porous separator and an electrolyte and the extent of storage of electrical energy is strongly based on the separation of charged species

at the electrode-electrolyte interface under the influence of applied electric field. Therefore, the physical properties of the active electrodes of the supercapacitor are very critical in developing high Farad supercapacitors, in which carbon aerogel plays significant role in enhancing the charge storage capacity of supercapacitors⁷. This is mainly because of its unique porous network structure of carbon aerogel, in which nano-meter sized carbon particles are interlinked in 3D network leading to high interfacial surface in the range of 300-1000 m²/g. Further, carbon aerogels also exhibited relatively large open porosity (50-80%) and the pore sizes are in the meso-porous regime, which enable use of internal surface of the electrodes by the electrolyte ions which make the EDLC a simpler, efficient and more reversible than in secondary batteries.



Fig. 1: Photograph of organic aerogel & carbon aerogel (left) & Computer controlled Supercritical Drying system (right)

Carbon Aerogel Preparation and development of Supercapacitors

Carbon aerogels were prepared from precursor organic aerogels by the pyrolysis of precursor in inert atmosphere. Precursor organic gels were synthesized through sol-gel polymerization/condensation of organic monomers by following the general procedure followed by supercritical drying of wet-gels^{1,8}. Fig. 1 shows the photograph of organic aerogel (RF aerogel) and corresponding carbon aerogel, developed indigenously.

The active electrodes for supercapacitor were fabricated by using optimized carbon aerogel composition in combination with organic binder by calendaring technique using locally fabricated

calendaring machine. The aerogel tapes of thickness 100 ± 20 mm were adhere to thin current collector sheet made of Al/Ag of thickness ~ 40 mm using carbon based conductive adhesive followed by thermal curing at $200-300^\circ\text{C}$ under N_2 using the atmosphere controlled electrode curing chamber shown in Fig. 2.

The aerogel supercapacitors of different values were fabricated by assembling the aerogel electrodes, separators, insulators as per the EDLC configuration by hand winding of components followed by impregnation of liquid electrolyte and sealing in cans of desired sizes. Instead of conventional aqueous based electrolyte, the organic electrolyte in non-aqueous medium was used in aerogel

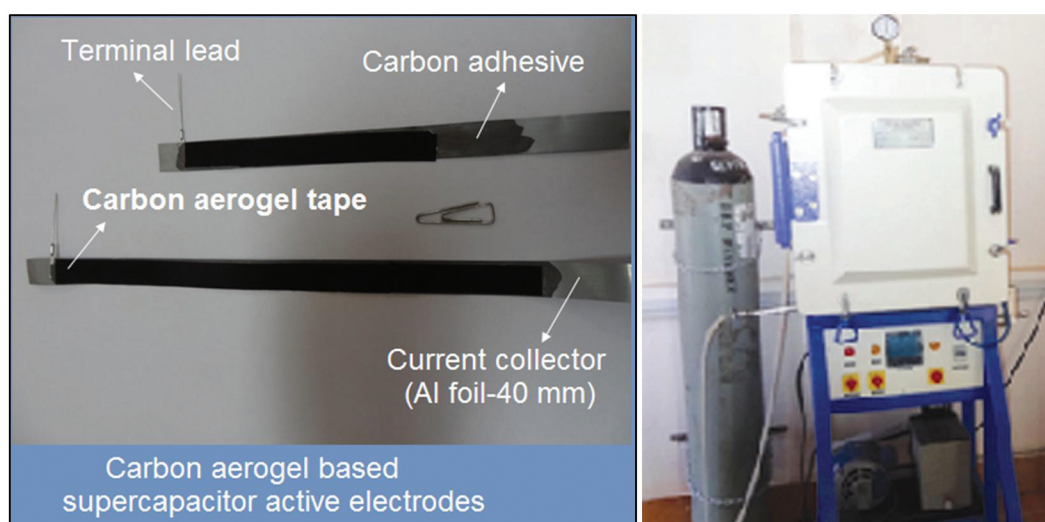


Fig. 2: Photograph of carbon aerogels based supercapacitor active electrodes (left) and the photograph of atmosphere controlled electrode curing chamber (right)

supercapacitors for storing higher amount joules by extending the working voltage to 2.5-2.7 V, as the energy $(E) = \frac{1}{2}CV^2$, where C is cell capacitance & V is working voltage of super capacitor. It is important to mention here that the electrolyte impregnated electrode wounds were sealed in cans immediately in order to avoid damage of cell from contamination due to moisture. Photographs of some aerogel supercapacitors of different capacitance (1 – 35 F), developed are shown in the Fig. 3.



Fig. 3: Photographs of carbon aerogel supercapacitors of capacitance 1 – 35 F.

Testing of Aerogel Super-capacitors

The electrical and electrochemical properties of the aerogel supercapacitors, such as cell capacitance, charge-discharge cycle (CDC), Equivalent Series

Resistance (ESR) etc. were studied using computer controlled super-capacitor testing system (SCTS) and electrochemical work station (EWS). Fig. 4 shows the photographs of in-house facilities of STCS & EWS.

Electrical properties of aerogel supercapacitors were studied by following constant current charge-discharge (CDC) techniques as per the International Standard EDLC testing procedure (IEC 62391-1), which displayed highly reversible charge/discharge patterns. Constant current charge discharge cycles of some selected aerogel super-capacitors, tested using SCTS are shown in Fig 5. The other electrical parameters of aerogel supercapacitors, such as cell capacitance, ESR, and energy release, etc. were obtained from the CDC patterns and some selected results are given in Table 1. Study of I-V characteristic of aerogel super-capacitors displayed characteristic rectangular shaped reversible cyclic voltammogram.

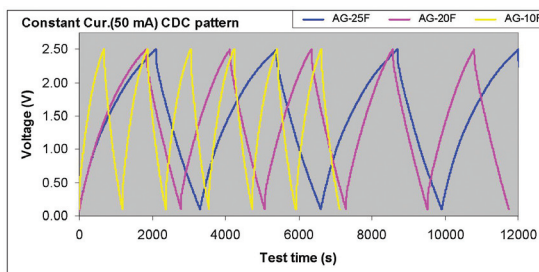


Fig. 5: Constant current (50 mA) charge-discharge pattern of 10F, 20 F and 25 F aerogel supercapacitors, studied by using SCTS.



Fig. 4: Photographs of Computer controlled Supercapacitor Test System (left) and Electrochemical Workstation, coupled with Frequency Response Analyzer (right)

Table 1: Electrical properties of some aerogel supercapacitors (10-35 F), fabricated from carbon aerogel and sealed in Al can using the tool for manual sealing

Sample code	Electrode size (L x W x T, mm)	Cell cap. (F)	Sp. cap. (F/g)	ESR (m Ω)	Energy density (WH/kg)
AG-478	400 x 25 x 0.09	10.81	43.23	325	2.33
AG-455	400 x 25 x 0.09	12.30	43.06	584	3.86
AG-497	400 x 25 x 0.14	20.30	62.88	128	5.19
AG-445 [#]	400 x 25 x 0.12	25.09 (25.25[#])	62.81	380 (147[#])	6.38
AG-507	400 x 28 x 0.13	30.57 (28.10^s)	61.14	105 (138[#])	6.04
AG-444 ^s	400 x 25 x 0.12	35.28 (35.30^s)	75.76	375	6.95

*values in parenthesis are the test results of end users; [#]Test result by third party end user-1 and ^sTest result of third party end user-2

Test report by third party end users showed very good capacitance tolerances (<2%). Third party end users also performed the electronic load test on Aerogel super-capacitors, which showed capability of withstanding higher electronic loads.

Supercapacitor Applications in Electronic Circuits

Applications of aerogel supercapacitor for demonstration in electronic circuits were developed. Some of application circuits, such as supercapacitor lighting LED lamp for bi-cycle tail light, running DC motor with fan, driving electronic toy-car with geared DC motor (Fig. 6) and aerogel super-capacitor stack demonstrating fast line-charging of emergency light with power LED (3W), and then glowing them (Fig. 7), etc. required electronic circuits for the specific applications were designed and fabricated for demonstration. These demonstration circuits

revealed that these small carbon aerogels supercapacitors are highly capable of storing high amount electric energy and then delivering power to electronic loads for specific applications.

Conclusions

This is complete indigenous technology for making carbon aerogels based Farad range super-capacitors up to 35 F using carbon aerogel as active electrode material. High surface area porous carbon aerogels of different compositions, suitable for EDLC electrode was also developed indigenously through sol-gel polymerization of organic monomers followed by carbonization. The material characterization of carbon aerogels was carried out thoroughly and they exhibited high specific surface area in the range of 300-800 m²/g with good electrical conductivities. Aerogel supercapacitors of different cell capacitance (upto 35 Farad) were



Fig. 6: Photograph some of the applications that demonstrated with the aerogels supercapacitors & required electronic circuits: (a) light LED Lamp, (b) running DC motor with fan and (c) running toy car with geared DC motor.



Fig. 7: Photograph of Aerogel supercapacitor powered fast charging Emergency Light having two 25F/ 2.5 V, 1-3W Power LED, which takes ~90 second for full charging and provide energy to light power LED for 30 min to 90 min, depending on LED lamp power (1-3W)

fabricated from carbon aerogel power by hand-winding the carbon aerogel based electrodes of different dimensions followed by sealing in cylindrical metal/plastic cell after impregnation of liquid electrolyte in it. Electrical and electrochemical characteristics of aerogel supercapacitors were studied by using the supercapacitor testing system (SCTS) and electrochemical workstation (EWS), which showed highly reversible charge-discharge patterns in constant current charging/discharge, and long cycle life. The aerogel supercapacitors fabricated showed the cell capacitance in the range 1-35 F, depending on the content of carbon aerogel and its electrode composition. Some demonstration electronic circuits were developed to show the probable applications of super-capacitors in electronics systems. Advancement to this work that is to make power-packs for industrial usage of several Farads of 5-24V and beyond are in progress.

Acknowledgements

Authors and the project team of C-MET thankfully acknowledge BRNS for funding this development partly under ATC-BRNS project (Sanction No. 2009/34/31/BRNS dated 22.10.2009). C-MET is also thankful to Dept. of Science & Technology and Dept. of Electronics & Information Technology for funding other projects on aerogels and providing financial support for the creating aerogel preparation and

fabrication of aerogel supercapacitors as well. We also thank M/s Tata Motors (Pune) and M/s Chheda Electricals & Electronics (P) Ltd. (Pune), for testing many samples, as prospective third party end users. The project team also acknowledges the encouragement and guidance of Shri B.B. Biswas (Fmr. Head Reactor Control Division-BARC), Shri G.P. Srivastava (Fmr. Director E & I Group), Dr R. K Bhandari (Fmr Director VECC-Kolkata), Dr. Srikumar Banerjee (Fmr Chairman DAE), Dr. K.R. Dayas (Director CMET-Thrissur), and Dr. R.K. Sinha (Chairman DAE).

Project Team: Stanly Jacob K, P A Abraham, Rani Panicker N and S. Rajasekharan of Aerogel Division, Centre for Materials for Electronics Technology (C-MET), Thrissur

Patents Filed

- 1) "Process of making carbon aerogel based electrode compositions and fast charge-discharge aerocapacitors for the high power electronic applications" Inventors: N.C. Pramanik et al (Indian Patent -Submitted on 18.11.2013)
- 2) "Method of producing high surface area conductive carbon aerogel for supercapacitor electrode" Inventors: N.C. Pramanik et al (Indian Patent-Submitted on 18.11.2013)

References

1. Ganeev RA, Naik PA, Chakera JA, Singhal H, Pramanik NC, Abraham PA, Ranipanicker N, Kumar M and Gupta PD "Carbon aerogel plumes as an efficient medium for higher harmonic generation in 50-90 nm range" *J. Opt. Soc. Am. B*, 28, (2011): 360-364.
2. B.E.Conway, *Electrochemical Supercapacitors: Scientific Fundamentals and Technological Applications*, Kluwer Academy, NewYork, 1999
3. Fischer U R S, Bockand V and Fricke J, "Carbon aerogel as electrode materials in supercapacitors" *J. Porous Mater.*, 4 (4), (1997): 281-285

4. Pekala RW (1989), "Organic aerogel from the polycondensation of resorcinol with formaldehyde" *J. Mater. Sci.*, 24(9), (1989): 3221-3227.
5. I. Tanahashi, A. Yoshida, A. Nishino, "Activated carbon fibre sheet as polarized electrodes of electric double layer capacitors" *Carbon* 28(4), 1990: 477-482
6. Kotz R and Carlen M, "Principles and applications of electrochemical capacitors" *Electrochimica Acta*, 45, (2000): 2483-24981
7. Shantanu Das and N C Pramanik, "Micro-structural roughness of electrodes manifesting as Temporal Fractional Order Differential Equation in supercapacitor transfer characteristics" *Intl. J. Mathematics & Computation*, 20, (2013): 94-113.
8. K. S. Rejitha, P. A. Abraham, N. Rani Panicker, K. Stanly Jacob and N. C. Pramanik*, "Role of catalyst on formation of resorcinol-furfural based carbon aerogels and its physical properties" *Advances in Nanoparticles*, 2, (2013): 99-103

Measurement of mechanical properties of a PHWR operated pressure tube using an in-house developed '*In situ* Property Measurement System (IProMS)'

S. Chatterjee, Sanjay Panwar, K. Madhusoodanan and P.K. Vijayan

Reactor Engineering Division

and

G.K. Mallik and V.D. Alur

Post Irradiation Examination Division

Abstract

In the field of alternate methods for estimation of properties of materials, cyclic ball indentation is an emerging technique. Reactor Engineering Division has developed an '*In situ* Property Measurement System (IProMS)', suitable for Zr-2.5Nb pressure tubes of 220 MWe PHWRs. It can be deployed for cyclic indentation trials inside a pressure tube at any axial location. Trials have been carried out at Post Irradiation Examination Division using IProMS in a reactor operated pressure tube, removed from Kakrapar Atomic Power Station-2 after 12.76 Full Power Years of operation. This report describes ball indentation technique and the results obtained from the trials carried out.

Introduction

Cyclic ball indentation is an emerging technique used for estimation of mechanical properties of materials. In this technique, a selected location on the surface of the test material is subjected to 8 to 10 loading and unloading indentation cycles using a tungsten carbide ball indenter. An analysis of the indentation load applied and the corresponding indentation depth produced using a methodology developed by Hagagg et. al. [1] gives an estimate of the mechanical properties of the test material. A material specific constant, independent of its condition is used to evaluate the properties. The systems available worldwide for doing ball indentation trials are mostly of fixed location based or are capable of doing the experiment on the outside surface of pipes. It may be noted that mechanical properties of many of the reactor components change during reactor operation due to nuclear radiation. Many times it may not be possible to remove the component from the reactor and, even in cases where the component can be removed, it is necessary

to bring it to radiological laboratories in heavily shielded flasks to prepare the specimens for measurement by conventional technique. The whole process, including the removal of the component is highly cumbersome and consumes large amount of radiation dose. In such cases, availability of a system which can be used under in-situ conditions to measure the properties would be highly appreciated. With this objective, an innovative system called, '*In situ* Property Measurement System (IProMS)' that can be located inside a tubular component to do the cyclic indentation trial has been developed by Reactor Engineering Division (RED) [2-6]. The system is specifically meant for pressure tubes of 220 MWe Pressurised Heavy Water Reactors (PHWRs). Periodic assessment of mechanical properties of pressure tube is a requirement for assessing its fitness for service [7]. Previously, the system has been qualified by conducting large number of trials inside Zr 2.5 wt% Nb pressure tubes having different known

mechanical properties. In the present work, indentation trials have been carried out at different axial locations inside a pressure tube Q10, removed from KAPS-2 (Kakrapar Atomic Power Station, Unit-2) after 12.76 Full Power Years (FPYs) of operation. The trials have been carried out at Post Irradiation Examination Division (PIED) of Bhabha Atomic Research Centre (BARC), where the tube has been shifted from reactor site for PIE studies. Description of IProMS, details of the trials carried out and the results obtained are highlighted in this report.

Description of IProMS

IProMS, shown in Fig. 1(a) basically consists of a tool head, a control and recording station and a pressurization module. Indentation is done using a tungsten carbide ball of diameter 1.5 mm, mounted at the tip of a piston. Indentation load is applied hydraulically from a remote location and the depth of indentation is measured using a LVDT, mounted on the piston. IProMS being installed inside a pressure tube spool piece is shown in Fig. 1(b).

Technique of measurement

The technique of measurement used in IProMS is based on an analysis of the data generated from multiple indentation cycles with intermittent partial unloading at the same location on the surface of the material being tested using a tungsten carbide ball. Each cycle consists of indentation, partial unload and reload sequences. The indentation load

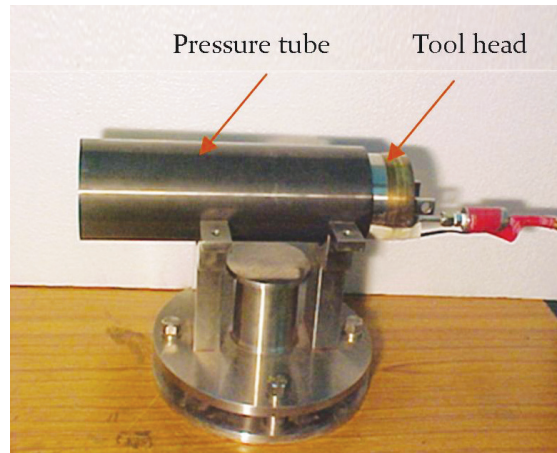


Fig. 1(b): IProMS inside pressure tube

and corresponding depth of indentation are recorded in a computer system during the test. Material properties like yield strength, ultimate tensile strength (UTS) and strain hardening exponent etc. are estimated from a post-processing of the data recorded.

Estimation of mechanical properties

The methodology used for estimation of mechanical properties from ball indentation test is described by Haggag [1]. From the data recorded during the test, values of peak load, total depth of indentation and plastic part of the depth of indentation corresponding to each unload cycle are used to estimate the mechanical properties. Schematic representation of ball indentation technique is shown in Fig. 2, the cyclic loading and unloading

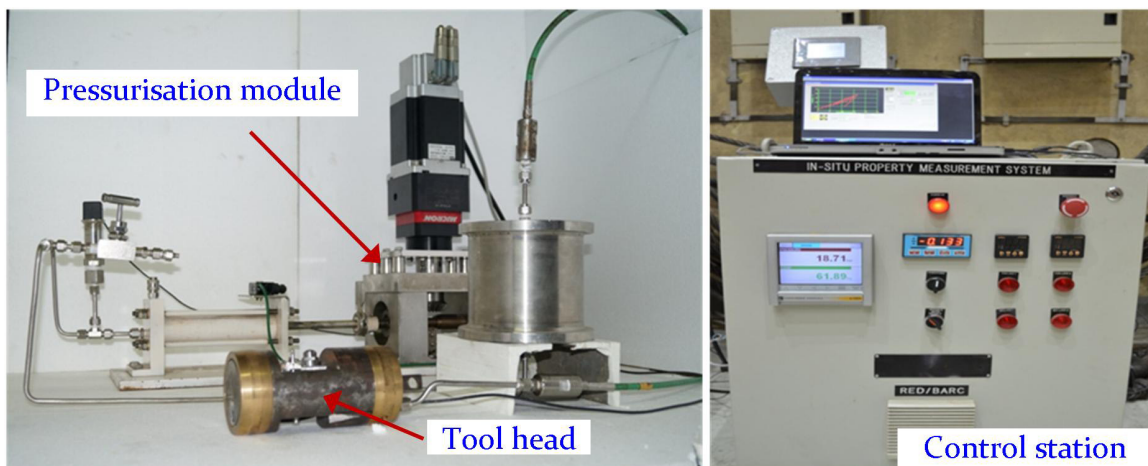


Fig. 1(a): IProMS tool head, pressurization module and control station

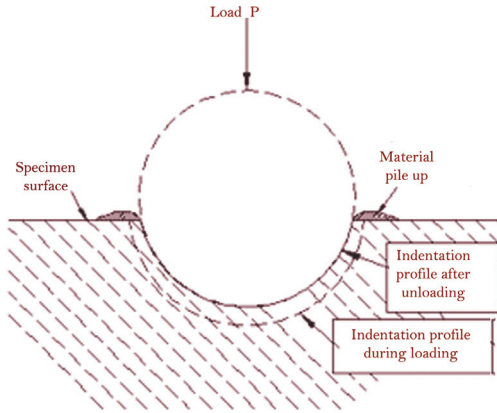


Fig. 2: Nomenclature involved in ball indentation

process is shown in Fig. 3 and the methodology of estimation of properties is described below:

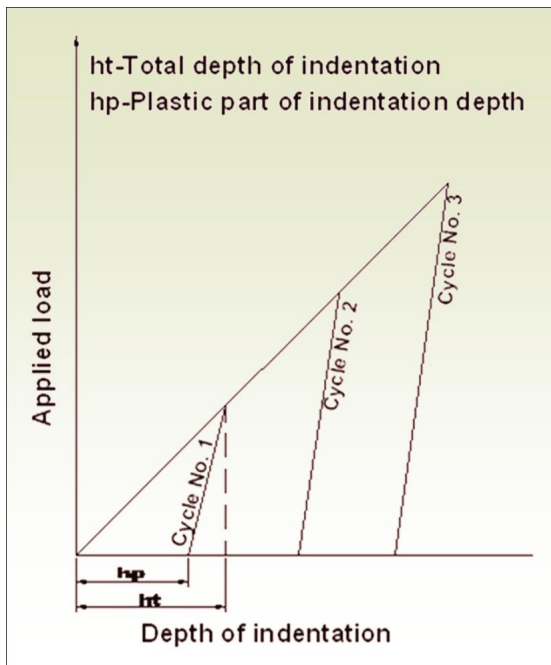


Fig. 3: Schematic of loading and unloading cycle

Methodology of estimation of properties

i) Estimation of yield strength

In order to estimate the yield strength, the Meyer’s equation (1) is fit to the data points corresponding to each unload cycle. A is called the proportionality constant and m is called Meyer’s coefficient. P is the load applied at the beginning of unload; D is

diameter of ball; \$d_t\$ is total indentation diameter at the beginning of unload [1].

$$\frac{P}{d_t^2} = A \left[\frac{d_t}{D} \right]^{m-2} \tag{1}$$

Values of A and m are derived from the fit of

$$\left(\frac{P}{d_t^2} \right) \text{ vs. } \left(\frac{d_t}{D} \right)$$

Yield strength is given by equation (2), in which \$\beta_m\$ is a constant specific to the material class [1].

$$\sigma_y = \beta_m A \tag{2}$$

ii) Estimation of ultimate tensile strength, UTS

In order to estimate the UTS, corresponding to each unload cycle, the values of true stress and true strain are estimated using equations (3) and (4).

$$\sigma_t = \frac{4P}{\pi d_p^2 \delta} \tag{3}$$

$$\epsilon_p = 0.2 \frac{d_p}{D} \tag{4}$$

where,

\$\sigma_t\$ is true stress, \$\epsilon_p\$ is true plastic strain, \$d_p\$ is diameter of indentation after unloading, given in equation (5) and \$\delta\$ is a material deformation parameter, estimated based on equation (7) [1].

$$d_p = \{0.5CD[h_p^2 + (d_p/2)^2]/[h_p^2 + (d_p/2)^2 - h_p D]\}^{1/3} \tag{5}$$

$$C = 5.47P[1/E_1 + 1/E_2] \tag{6}$$

where,

\$h_p\$ is the depth of indentation after unloading, \$E_1\$ is Young’s modulus of indenter material and \$E_2\$ is Young’s modulus of test material.

$$\delta = \begin{cases} 1.12 & \phi \leq 1 \\ 1.12 + \tau \ln \phi & 1 < \phi \leq 27 \\ \delta_{max} & \phi > 27 \end{cases} \tag{7}$$

$$\phi = \epsilon_p E_z / 0.43 \sigma_t \quad (8)$$

$$\delta_{max} = 2.87 \alpha_m \quad (9)$$

$$\tau = (\delta_{max} - 1.12) / \ln(27) \quad (10)$$

where,

α_m is a strain rate sensitivity parameter, and is taken as 1.0 [1].

Power equation (11) is fit to the values of true stress and true strain.

$$\sigma_t = k \epsilon_p^n \quad (11)$$

The values of strength coefficient k and strain hardening exponent n , obtained by fitting equation (11) to the estimated values of σ_t and ϵ_p are used to estimate the value of UTS using equation (12).

$$UTS = k(n/e)^n, e \approx 2.71 \quad (12)$$

iii) Material hardness

Material hardness in BHN is given by equation (13) [1].

$$HB = \frac{2P_{max}}{\pi D(D - (D^2 - d_{pf}^2)^{1/2})} \quad (13)$$

where,

P_{max} is the maximum load applied during the last unload cycle and d_{pf} is the diameter of indentation after final unloading.

Trials inside irradiated pressure tube

As the radioactivity level of the pressure tube is high, to reduce the exposure to personnel, trials were carried out by locating the pressure tube inside a shielded flask and restraining its movement. Against the standard procedure of polishing of the surface before ball indentation tests, the trials were done at different axial locations in as received surface

condition of the pressure tube. An extension pipe having the axial test locations marked, carrying the cables of LVDT and hydraulic hose was attached to the tool head and it was guided through the pressure tube. The measurement operation in progress is shown in Fig. 4(a) and 4(b).

Results of analysis



Fig. 4(a): IProMS tool head being inserted inside the pressure tube Q10 at PIED, BARC



Fig. 4(b): IProMS tool head being inserted inside the pressure tube Q10 at PIED, BARC

Variation of load vs. indentation depth data acquired from inlet end, outlet end and middle portion of the irradiated pressure tube is shown in Fig. 5. Properties estimated from indentation tests carried out at different axial locations of the pressure tube are tabulated in Table 1. In Table 1, the value of yield strength is derived from equation (2), k and n are derived from equation (11), UTS is derived from equation (12) and hardness is derived from equation (13). The variation of properties estimated along

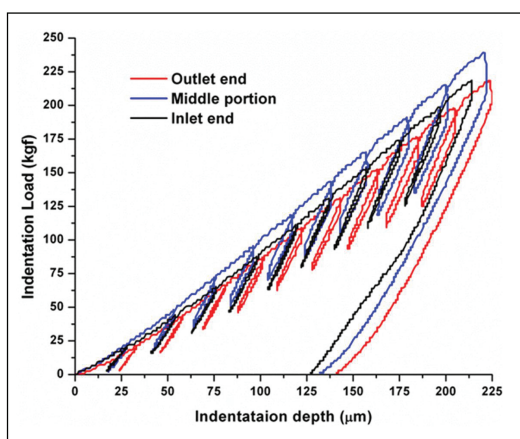


Fig. 5: Comparison of load-deformation curves recorded during tests on Q10 pressure tube at different locations

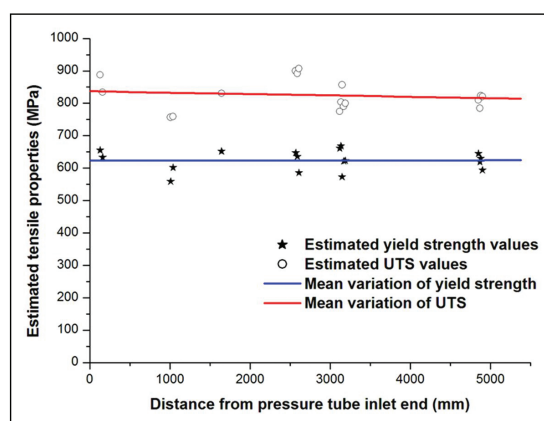


Fig. 6: Variation of IProMS estimated tensile properties along the length of Q10 pressure tube and the mean estimate

the length of the pressure tube along with the mean estimate is given in Fig. 6 and Fig. 7. The IProMS estimated true stress vs. true plastic strain data

acquired from irradiated and a typical unirradiated pressure tube is shown in Fig. 8.

Discussion

Table1: IProMS Estimated properties of irradiated pressure tube Q10 of KAPS-2

Test No.	Distance from pressure tube inlet end (mm)	Estimated mechanical properties from IProMS				
		Yield strength (MPa)	UTS (MPa)	Hardness (BHN)	Strain hardening exponent (n)	Strength coefficient, k (MPa)
1	130	655	888	277	0.103	1244
2	160	633	834	269	0.099	1158
3	1010	559	757	251	0.12	1101
4	1040	602	759	251	0.089	1029
5	1645	652	831	265	0.091	1132
6	2570	647	900	282	0.11	1281
7	2590	636	892	280	0.111	1272
8	2610	586	907	282	0.131	1350
9	3120	661	775	272	0.073	1009
10	3135	668	804	267	0.078	1061
11	3150	573	857	270	0.13	1272
12	3170	622	790	263	0.093	1081
13	3190	623	800	260	0.093	1095
14	4850	645	810	259	0.084	1085
15	4870	619	785	253	0.088	1062
16	4880	630	823	265	0.096	1135
17	4900	594	821	259	0.105	1155

Material constants: $\alpha_m = 1$, $\beta_m = 0.2652$ [5]; Young's modulus of Zr-2.5Nb = 95 GPa [8];

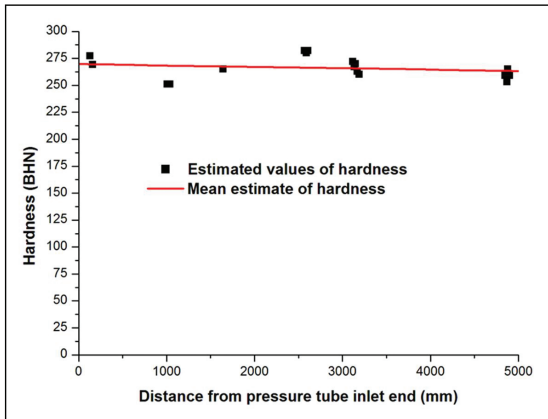


Fig. 7: Variation of IProMS estimated hardness along the length of Q10 pressure tube and the mean estimate

An innovative system based on cyclic ball indentation technique has been used to estimate the mechanical properties of an irradiated pressure tube Q10, removed from KAPS-2 after 12.76 FPYs of operation. It can be observed from Fig. 5 that the slope of load-indentation depth data acquired from the middle portion of the pressure tube is more compared to that acquired from its ends. Figures 6 and 7 show the variations of YS, UTS and hardness along the length of the irradiated pressure tube showing highest values at its middle portion. Based on the data given in Table 1, the average yield strength of the pressure tube is 620 MPa and the UTS is 840 MPa, with standard deviations of 31 MPa and 49 MPa respectively. It is to be noted that the test surface of the pressure tube was not specially prepared before the tests, which is the procedure normally followed. Figure 8 shows the comparison between the true stress-true plastic strain data of the tests carried out on irradiated pressure tube Q10 and a typical unirradiated pressure tube using IProMS. It can be observed from Fig. 8 that there is a 20 to 30% increase in strength of the pressure tube after irradiation. The mean values of strain hardening exponent (n) of irradiated and unirradiated pressure tube based on the data shown in Fig. 8 are 0.164 and 0.168 respectively and the mean values of strength coefficient (k) for the same are 1395 MPa and 1098 MPa respectively. It is to be noted that IProMS tests have been carried out on irradiated

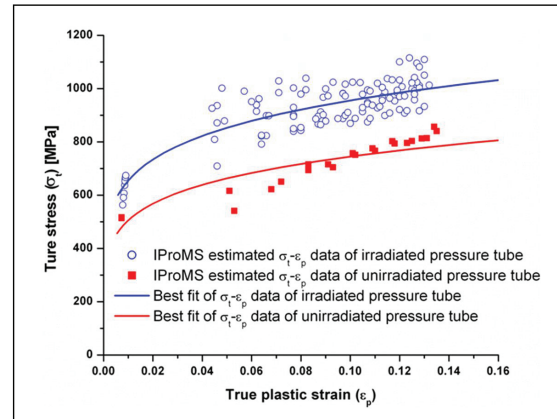


Fig. 8: Comparison of IProMS estimated true stress vs. true plastic strain acquired from irradiated and unirradiated pressure tube

pressure tube Q10 all along its length of about 5 m, whereas for the tests on unirradiated tube, a spool piece of about 200 mm length has been used. Hence, the scatter in true stress-true plastic strain data is observed to be more for the tests carried out on irradiated pressure tube than that of the unirradiated tube.

Conclusion

An innovative system called 'In situ Property Measurement System (IProMS)' developed in-house by Reactor Engineering Division has been used for measurement of mechanical properties of an irradiated pressure tube removed from KAPS-2 after 12.76 FPYs of operation. Properties have been estimated at different axial locations of the pressure tube, by keeping the tube inside a shielded flask at Post Irradiation Examination Division, BARC. The results show 20 to 30% increase in mechanical properties of the pressure tube after 12.76 FPYs of irradiation, as compared to that of a typical unirradiated pressure tube. As this was the first attempt towards such an activity of measurement of mechanical properties of irradiated pressure tube using remotely operable IProMS, the properties estimated need to be validated with that derived from conventional tensile tests to be done on samples prepared from different axial locations of the tube. More tests need to be done on pressure tubes irradiated for different time periods for further optimization of the test procedure.

Acknowledgement

The authors are grateful to Shri K.K. Vaze, Former Director, Reactor Design & Development Group and Shri S. Anantharaman, Head, PIED for their support and encouragement in the execution of the job. Authors are also grateful to all the technicians of RED and PIED who are associated with the experimental programme.

References

1. Haggag. F.M., 'In-Situ Measurements of Mechanical Properties Using Novel Automated Ball Indentation System', ASTM STP 1204, pp 27-44, 1993.
2. Chatterjee S., Madhusoodanan K., Panwar Sanjay and Rupani B.B., "Design of in-situ property measurement system", *International conference on Advances in Mechanical Engineering*, Fatehgarh Sahib, Punjab, India (2006) M-I:27, 172-177.
3. Chatterjee S., Madhusoodanan K., Panwar Sanjay and Rupani B. B., "In-situ measurement of mechanical properties of structural components using cyclic ball indentation technique", Theme meeting on modern developments and practices in mechanical testing of structural materials, Bhabha Atomic Research Centre, Trombay, (2007) 121-126.
4. Murty K.L., Mathew M.D., Wang Y., Shah V.N., Haggag. F.M., *International Journal of Pressure Vessels and Piping* 75 (1998): 831-840.
5. Chatterjee S., Madhusoodanan K., Dr. Singh R.N., Panwar Sanjay and Kayal J.N., "Non-destructive measurement of mechanical properties of Zr 2.5 wt% Nb pressure tube", *21st International conference on Structural Mechanics in Reactor Technology (SMiRT 21)*, New Delhi, India, (2011) Div-VIII.
6. Chatterjee S., Madhusoodanan K. and Kayal J. N., "Finite element simulation of cyclic ball indentation on Zr 2.5 wt% Nb alloy and assessment of the residual stress produced", *6th International Conference on Creep, Fatigue and Creep-Fatigue Interaction (CF-6)*, Mamallapuram, India, (2012) 716-725.
7. In-service inspection plan for Zr 2.5% Nb coolant channel assemblies of 220 MWe reactors, document No. NPCIL/31110/CC/M/2011/101, dated 02/05/2011.
8. Northwood D. O., London I.M., Bahen L. E., "Elastic Constants of Zirconium Alloys", *Journal of Nuclear Materials* 55 (1975) 299-310.

Numerical Simulations to Evaluate Different Approaches for scaling up of Packed Bed Membrane Reactor for HI Decomposition

Nitesh Goswami, Soumitra Kar, R.C. Bindal and P.K.Tewari

Desalination Division

and

K.K. Singh

Chemical Engineering Division

Abstract

Evaluation of different approaches to scale up PBMR (Packed Bed Membrane Reactor) for HI decomposition has been carried out using numerical simulations. Numerical simulations involve coupled solution of momentum, energy and species transport equations. The results suggest that, to produce hydrogen at large scale, it is better to use several small diameter reactors in parallel than using a single large diameter reactor or a single longer reactor.

Introduction

Extensive research is being carried out in BARC by different groups of researchers for addressing various critical issues associated with production of hydrogen by thermochemical splitting of water by IS process. Efforts are being made for the development of membrane-based processes applicable to HI_x processing stream. In this regard, Desalination Division, BARC is associated with the development of silica-based membrane reactor for enhancement of equilibrium decomposition of HI. An attempt has been made to develop silica membrane [1] on alumina support with graded porosity using sol-gel processing. A prototype membrane reactor has also been developed in-house.

IS thermochemical process is one of the promising processes of hydrogen production amongst all the alternatives available keeping in view of the predicted thermo-chemical efficiency and possibility to couple it to a high temperature nuclear reactor [2]. The IS process consists of following reactions:



The third reaction is HI decomposition reaction in which H₂ and I₂ are produced. Activated charcoal is one of the potential catalysts for this reaction. H₂ is the product, I₂ is recycled into the Bunsen reaction. In the overall reaction, H₂O is decomposed into H₂ and O₂. The equilibrium conversion of decomposition of HI is very low which increases the costs and efforts involved in production of H₂ from this cycle. Kar et al. [3] cited that the low decomposition ratio leads to reduction in the thermal efficiency of the cycle. One of the methods to enhance the decomposition of HI could be based on hydrogen permselective membrane reactor. A membrane reactor is a single unit integrating both reaction and membrane-based separation. It can also be termed as membrane-based reactive separation. Several studies on computational fluid dynamics (CFD) modeling of the membrane reactors have been reported in literature. CFD modeling of ammonia cracking inside a catalytic membrane reactor has been reported by Carlo et al. [4]. Marin et al. [5] reported a 2D membrane reactor model involving momentum, mass and energy transport. The model was validated with experimental data of the methane steam reforming reaction. Smith et al. [6] analyzed the performance of a membrane reactor

for low temperature water gas shift reaction using CFD simulations. While the CFD modeling of membrane reactors for other reactions do provide useful information, the results and conclusion obtained for one reaction may not be applicable directly for another reactions due to change in kinetics, heat effects and physical properties. The objective of this paper is to evaluate different approaches for scaling up a PBMR for HI decomposition using the numerical simulations.

Computational Approach

A commercial package COMSOL Multiphysics has been used to carry out the numerical simulations which involve solution of momentum, energy and species transport equations. Brinkman equation and Maxwell-Stefan equation have been used for momentum and mass transport, respectively. For energy transport, both conductive and convective heat transfer have been considered. Variation of properties like viscosity, density, heat capacity etc. with temperature and pressure are taken into account in the model by using the suitable equations.

For HI decomposition which is an endothermic reaction, a Langmuir-Hinshelwood type rate equation, proposed by Oosawa et al [7] for the catalytic decomposition of HI using an active carbon catalyst, is used for carrying out the simulations. The relevant expressions are given by Eqs. (4) – (8)

$$r_{HI} = -k p R_{HI} \tag{4}$$

$$R_{HI} = \frac{x_{HI}}{1 + K_{I_2} P x_{I_2}} - \frac{\sqrt{x_{H_2} x_{I_2}} (1 + K_{I_2} P \frac{\phi_e}{2})}{K_p (1 + K_{I_2} P x_{I_2})^2} \tag{5}$$

$$k = 1.58 \times 10^{-1} \exp\left(-\frac{E_{a1}}{RT}\right) \tag{6}$$

$$K_{I_2} = 5.086 \times 10^{-11} \exp\left(-\frac{E_{a2}}{RT}\right) \tag{7}$$

Where, p is pressure, x is mole fraction, r_{HI} is the rate of reaction ($\text{mol}/\text{m}^3 \cdot \text{s}$), K_{I_2} is coefficient of adsorption of iodine, E_{a1} is $34.31 \times 10^3 \text{ J/mol}$ and E_{a2} is $-86.66 \times 10^3 \text{ J/mol}$ [8]. Φ_e is the equilibrium

conversion (0.21 at 700K). The equilibrium constant, K_p for the decomposition of HI is obtained by the free energy values given in the JANAF [9] using the following equation:

$$K_p = \exp\left(-\frac{\Delta G}{RT}\right) \tag{8}$$

Where, ΔG is 11.5 kJ/mol at 700 K.

Grid independence test is done to decide the mesh density to be used for carrying out the simulations. The computational approach adopted in this study has been validated using the experimental data reported for steam reforming of methanol in a packed bed tubular reactor [10]. Complete details of the computational approach used in numerical simulations are reported elsewhere [11].

Results

Three approaches to scale up from a small-scale reactor are possible. In the first approach several identical small-scale reactors can be placed in a parallel flow arrangement. In the second approach, the small-scale reactor can be made longer to provide the same residence time as in the small-scale reactor. In the third approach, the diameter of the small-scale reactor can be increased to provide the same residence time as in the small scale reactor. All the three approaches were evaluated using two-dimensional numerical simulations. Other parameters which affect the performance of the reactor e.g. reactor wall temperature, feed temperature, feed composition, outlet pressure, porosity of the bed, diameter of the particles and membrane permeability were kept same. The values are given in Table 1.

A small-scale PBMR of 1.5 m length and 0.1 m diameter having feed velocity 0.01 m/s was considered as the base case. Scale up to achieve 2 times the feed velocity in small-scale reactor was considered. The first simulation was for the small-scale reactor itself. In the second simulation, a PBMR (longer reactor) with length and feed velocity twice of that of the small-scale reactor was considered. In

Table 1: Operating parameters and properties of the packed bed and membrane

Wall temperature (T_w)	700 K
Feed temperature (T_f)	600 K
Outlet pressure (p_0)	1 atm
Membrane permeability (P_0)	$1.3 \times 10^{17} \text{ mol Pa}^{-1} \text{ m}^{-2} \text{ s}^{-1}$
Packed bed porosity (ϵ)	0.3
Mole fractions in feed	HI: 0.99; I ₂ : 0.001, rest H ₂
Particle diameter	1 mm

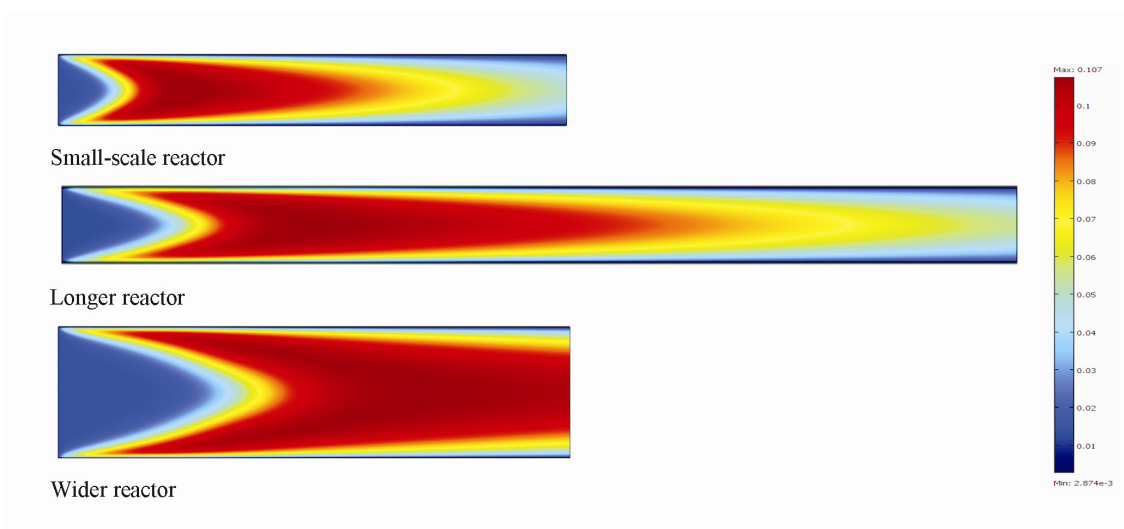
the third simulation, a PBMR (wider reactor) having width twice of that of the small-scale PBMR but having the same feed velocity and length as the small-scale PBMR was considered. Fig. 1 shows the variation of mole fraction of H₂ inside the reactors as predicted from numerical simulations. Fig. 2 shows the temperature field inside the reactors as obtained from numerical simulation. Table 2 compiles important data obtained from the numerical simulations.

Discussion

The hydrogen mole fraction profiles in Fig. 1 show that very less hydrogen is present in the central zone near the inlet. This is because the feed in the central zone takes some distance to feel the effect of wall

temperature and reach the reaction temperature. This distance increases with increase in feed velocity and reactor width, as seen in Fig. 2. This causes the average temperature in the wider PBMR to be lower than in the small-scale PBMR which causes the average reaction rate and conversion be lower in the wider reactor than in the small-scale reactor. Thus, two small-scale reactors in parallel is a

better scale up approach than having a single wider reactor. Despite longer preheating length due to high feed velocity, the average rate of reaction in the longer PBMR is more than that in the small-scale PBMR. The pressure drop is very high in the longer PBMR. Since the outlet pressure is maintained constant, a higher pressure drop causes average pressure inside the longer PBMR to be higher. The higher pressure causes average hydrogen permeation flux and average reaction rate to be higher in the longer PBMR than in the small-scale reactor. Despite being wider, pressure drop in the wider PBMR is more than that in the small-scale PBMR. This is due to higher viscosity of the reaction mixture owing to lower mean temperature in the wider PBMR. Since

**Fig. 1: Mole fraction profile of H₂ inside the PBMRs**

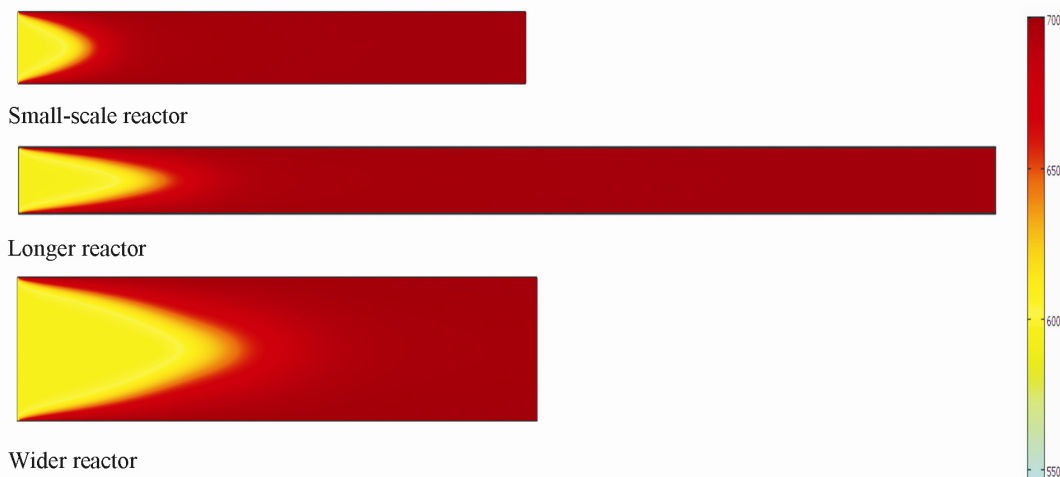


Fig. 2: Temperature field inside the PBMRs (scale in Kelvin)

Table 2: Important data resulting from numerical simulations

Reactor	Average temperature (K)	Average reaction rate (mol/m ³ .s)	Pressure drop (N/m ²)	Average H ₂ permeation flux (mol/m ² .s)	Conversion
Small-scale PBMR	689.14	0.116	2717	7.64×10 ⁻⁵	0.834
Longer PBMR	688.69	0.123	11888	7.85×10 ⁻⁵	0.819
Wider PBMR	668.96	0.086	4519	7.68×10 ⁻⁵	0.608

the outlet pressure is same for all the reactors, average pressure in the wider PBMR is more than the average pressure in the small-scale PBMR. This causes the average permeation flux to be slightly higher in the wider PBMR than in the small-scale PBMR despite of the conversion being more in the small-scale PBMR. Though the average reaction rate in the longer PBMR is more than that in the small-scale PBMR, conversion in the longer PBMR is lower than that in the small-scale PBMR. Since pressure drop is more in the longer PBMR, for the same outlet pressure and same feed velocity, the density of the feed mixture and hence the mass flux at the inlet of the longer PBMR is more than the same for the small-scale reactor. The increased reaction rate in the longer PBMR is not able to offset the increased mass flux causing the conversion to be smaller in

the longer PBMR than the small-scale PBMR despite of higher average reaction rate in the longer PBMR.

The pressure drop inside the small-scale PBMR is lower and the conversion is slightly higher than that in the longer PBMR. Hence, using parallel small-scale PBMRs reactors is a better scale-up alternative than using a longer PBMR. Due to very small conversion, using a wider PBMR is not an appropriate option for scaling up.

Conclusion

Different approaches for scale up of PBMR for HI decomposition have been studied by the numerical simulations. A small-scale PBMR reactor gives 83.4% conversion. The conversion obtained in the longer PBMR having twice the feed velocity of the small-scale PBMR is 82%. The wider PBMR having

width twice that of the small-scale PBMR gives only 61% conversion. The conversion obtained in the longer PBMR is almost same as that obtained in the small-scale PBMR but pressure drop is much higher. Hence, it is concluded that to produce hydrogen at large scale, it is better to use several small-scale PBMRs in parallel than using a single longer PBMR or a single large diameter PBMR.

Acknowledgement

Authors are thankful to Head, ChED, BARC for allowing access to computational resources.

References

1. S. Kar, R.C. Bindal, S. Prabhakar, P.K. Tewari, S. Ramanathan, J. Nuwad, et al., Membrane development for applications in hydrogen production using the sulphur-iodine thermochemical route, *Int J Nucl Hydrogen Production Appl*, 2(2011), 227-236
2. M. Nomura, S. Kasahara, H. Okuda and S. Nakao, Evaluation of the IS process featuring membrane techniques by total thermal efficiency, *Int. J. Hydrogen Energy*, 30 (2005), 1465-1473
3. S. Kar, R.C. Bindal, S. Prabhakar and P.K. Tewari, The application of membrane reactor technology in hydrogen production using S-I thermochemical process: A roadmap, *Int. J. Hydrogen energy*, 37 (2012), 3612-3620
4. A.D. Carlo, A Dell'Era, Z D Prete, 3D simulation of hydrogen production by ammonia decomposition in a catalytic membrane reactor, *Int. J. hydrogen energy* 36(2011), 11815-11824
5. P. Marín, Y. Patinõ, F. V. Díez, S Ordoñez, Modelling of hydrogen perm-selective membrane reactors for catalytic methane steam reforming; *Int. J. hydrogen energy* 37(2012), 1843 – 18445
6. R.J.B. Smith, L. Muruganandam, S.M. Shekhar, CFD analysis of water gas shift membrane reactor, *Chem. Engg. Research and Design* 89 (2011), 2448–2456
7. Y. Oosawa, T. Kumagai, S. Mizuta, W. Kondo, Y. Takemori, K. Fujii, Kinetics of the catalytic decomposition of hydrogen iodide in the magnesium–iodine thermochemical cycle, *Bull. Chem. Soc. Jpn.*, 54 (1981), 742-748.
8. G-J. Hwang and K. Onuki, Simulation study on the catalytic decomposition of hydrogen iodide in a membrane reactor with a silica membrane for the thermochemical water-splitting IS process, *Journal of membrane science* 194 (2001) 207-215.
9. JANAF Thermochemical Tables, Dow Chemical Company, Midland, 1977.
10. A. Karim, J. Bravo, A. Datye, Nonisothermality in packed bed reactors for steam reforming of methanol, *Appl. Catal. A: General*, 282 (2005), 101–109
11. N. Goswami, Evaluation of Membrane Reactor for HI decomposition studies, M.Tech. Thesis (2014), Homi Bhabha National Institute, Mumbai, India.

Nisargruna Plant Inaugurated at RRCAT Campus, Indore

Chairman, AEC and Secretary DAE Dr. R. K. Sinha inaugurated 1MT capacity Nisargruna biogas plant at RRCAT campus, Indore on July 26, 2014. The construction and installation of the Nisargruna plant was completed in a record 66 days. The plant is located opposite to RRCAT guest house.

The biogas generated in the process is used in guest house canteen. The manure will be used in vegetable garden which will be developed soon around the plant. It is encouraging to note the intense awareness campaign taken up by RRCAT Nature Club and AEC School in the campus. The motivation and inspiring leadership of RRCAT Director Dr. P. D. Gupta is instrumental in bringing a sea change in the attitude of residents. The students of AEC School visited every house and campaigned for segregation. The waste segregation level achieved is quite



Dr. R. K. Sinha inaugurating Nisargruna plant at RRCAT campus, Indore. Also seen in the picture among others is Dr. P. D. Gupta, Director, RRCAT

impressive. The feedback received from almost all the residents has also helped in taking the initiative ahead by leaps and bounds.



Nisargruna plant at RRCAT campus, Indore.

Conference on “75-years of Nuclear Fission: Present status and future perspectives”

Nuclear fission was discovered 75 years ago and is considered to be one of the most important scientific discoveries in basic and applied nuclear research. It has played a key role in the understanding of statistical and dynamical properties of nuclei, in the production of nuclear power, development of nuclear instrumentation and evolution of other related fields. In order to commemorate this occasion, a conference on “75 years of Nuclear Fission: Present status and future perspectives” was organized by Nuclear Physics Division, Bhabha Atomic Research Centre, Mumbai during May 8-10, 2014 at the Nabhikiya Urja Bhavan Auditorium, Anushaktinagar. The conference was sponsored by the Board of Research in Nuclear Sciences (BRNS). The main goal of the conference was to review the progress in the understanding of nuclear fission during past 75 years and also to indicate the direction of future research in fission. Nuclear fission occupies a prominent place in the context of global energy resources, and has

given impetus to scientists and engineers to look at advanced reactors for the production of cost effective nuclear power.

The conference provided a scientific forum for participants to discuss their work and interact with other researchers in the field of nuclear fission and related areas. It provided a wide exposure of nuclear fission studies using advanced reactors, accelerators and detector systems, spanning a wide range of topics of current interest. There was an enthusiastic response from the participants across the globe to discuss various aspects of nuclear fission. There were about 200 participants in the conference including 17 from abroad. The one-page abstracts from 45 invited speakers and 56 contributed papers for poster presentations were published in an abstract book. The research papers covered topics in the field of fission process, fission fragment spectroscopy, radiochemical studies in fission, cluster radioactive decay, superheavy element studies and various



From Left: Dr. S.S. Kapoor, Prof. V.S. Ramamurthy, Dr. R.K. Sinha, Dr. V.M. Datar, Dr. D.C. Biswas



A group photograph of the participants of Fission75 conference

applications of fission data. The role of nuclear fission in the design of advanced nuclear reactors, radioactive ion beam production and development of sophisticated experimental techniques were highlighted.

In his welcome address Dr. V.M. Datar, Chairman of the organizing committee, mentioned about the goals of the conference in the context of nuclear fission research programme in BARC. Prof. V.S. Ramamurthy, Director, National Institute of Advanced studies (NIAS) and former Secretary, DST, delivered the keynote address. He emphasized the relevance of basic research in the understanding of nuclear fission processes and its application in various fields. Dr. R.K. Sinha, Chairman, Atomic Energy Commission inaugurated the conference and highlighted the progress of nuclear science and engineering since the discovery of fission in 1939. He has made special mentioned of the role of fission for the production of nuclear energy in the service

of mankind. Dr. S.S. Kapoor, INSA Honorary scientist and former Director, Physics Group, BARC gave an overview of the nuclear fission research and mentioned that it is one of the landmark discoveries in Nuclear Physics. He presented some of the exciting results on superheavy elements and also discussed the possibility of accelerator driven sub-critical reactor system for nuclear power production. In the inauguration function, the formal vote of thanks was given by Dr. D.C. Biswas, Convener of the conference.

Many eminent scientists from BARC and Indian Universities, who have made significant contributions in the fields of nuclear fission for last many decades, participated in the conference. There was a special reminiscences session on May 09, 2014, to recollect their involvement in the growth and development of research activities on nuclear fission and related fields in India. Dr. S. Kailas, former Director, Physics Group, BARC delivered the summary talk of the conference.

BARC Scientists Honoured

Name of the Scientist : **Kinshuk Dasgupta**
Affiliation : Rare Earths Development Section, Materials Group, BARC
Name of Award/Honour : Ambuja Cement Best PhD (Tech.) Thesis Award instituted by the Institute of Chemical Technology, Mumbai
Title of the thesis : "Studies in Synthesis and Characterization of Carbon Nanotubes by Catalytic Chemical Vapor Deposition"

Name of the Scientist : **Saurav Kumar Guin**
Affiliation : Fuel Chemistry Division, BARC
Name of Award/Honour : 1st Poster Prize
Title of the Paper : An Insights into the Electrocatalysis of U(VI) on Gold Nanoparticles (AuNPs)
Presented at : "ECHEMS 2014: Electrochemistry in Molecular Understanding" held at Wells in United Kingdom during June 17-20, 2014

Name of the Scientist : **P. Suprasanna**
Affiliation : Nuclear Agriculture & Biotechnology Division, BARC
Name of Award/Honour : Prof. H.S. Srivastava Memorial Lecture Award
Presented at : Doon University, Dehradun



Calabash Tree at BARC

Edited & Published by:
Scientific Information Resource Division,
Bhabha Atomic Research Centre, Trombay, Mumbai 400 085, India
BARC Newsletter is also available at URL:<http://www.barc.gov.in>